Toroidal dipole and magnetic multipole excitations from the same nanostructure with different direction of electric dipole emitters

Citation: Applied Physics A. 2020 Feb 03;126(3):150

As Published: https://doi.org/10.1007/s00339-020-3325-y

Publisher: Springer Berlin Heidelberg

Persistent URL: https://hdl.handle.net/1721.1/131558

Version: Author's final manuscript: final author's manuscript post peer review, without publisher's formatting or copy editing

Toroidal dipole and magnetic multipole excitations from the same nanostructure with different direction of electric dipole emitters

Cite this article as: Yudan Sun, Haiwei Mu, Jingwei Lv, Qiang Liu, Chao Liu, Jiudi Sun, Tao Sun and Paul K. Chu, Toroidal dipole and magnetic multipole excitations from the same nanostructure with different direction of electric dipole emitters, Applied Physics A https://doi.org/10.1007/s00339-020-3325-y

Toroidal dipole and magnetic multipole excitations from the same nanostructure with different direction of electric dipole emitters

Yudan Sun[1,2], Haiwei Mu[1] , Jingwei Lv[1] , Qiang Liu[1], Chao Liu[1*], Jiudi Sun[1], Tao Sun[3] and Paul K. Chu[4]

Received XX Month XXXX; revised XX Month, XXXX; accepted XX Month XXXX; posted XX Month XXXX (Doc. ID XXXXX); published XX Month XXXX

Abstract

The toroidal dipole (TD) and magnetic multipole with optical response from high-index dielectric nanostructures are emerging optical nanostructures especially in the visible spectrum. However, interference of the involved multipoles is generally overlooked in the ultraviolet (UV) region. In this work, a novel nanostructure which can achieve excitations of TD, magnetic quadrupole (MQ) and magnetic dipole (MD) is demonstrated by simply changing the direction of the electric dipole emitters (EDs) in the wavelength range between 230 and 430 nm. Near perfect TD and magnetic excitations from the same structure are accomplished and our results also provide insights into the design and application of light nanoantennas, spectroscopy, and ultrafast light emitting devices.

1. Introduction

Nanoantennas have drawn a great deal of attention due to the ability to support highly efficient local surface plasmon resonance and confined electromagnetic field enhancement and have great potential in applications in biology, chemistry and physics such as biochemical sensors, light harvesting devices, and high-density optical data storage [1-6]. It is found that the toroidal dipole （TD） and magnetic multipole can be supported in plasmonic nanoantennas [7]. The TD is defined as the peculiar primary current excitation corresponding to the current circulating along the meridians (so-called poloidal currents) of the ideal torus.

ChaoLiu
msm-liu@126.com
1 School of Electronics Science, Northeast Petroleum University, Daqing 163318, P.R. China.
2 College of Mechanical and Electrical Engineering, Daqing Normal University , Daqing 163712,P.R.China.
3 Media Lab, Massachusetts Institute of Technology, Cambridge, MA02139, USA.
4 Department of Physics, Department of Materials Science and Engineering, and Department of Biomedical Engineering, City University of Hong Kong, Tat Chee Avenue, Kowloon, Hong Kong, China.

TDs provide physically significant contributions to the basic characteristics of matter including absorption, dispersion and optical activity. TD excitation also exist in free space as spatially and temporally localized electromagnetic pulses propagating at the speed of light and interacting with matter. Existence of the static TD has been studied and its importance in many solid-state systems has been discussed in ferromagnetic [8] and ferroelectric nanomaterials [9] as well as microstructures [10-12]. Owing to the weak coupling of toroidal multipole with incident electromagnetic wave, TDs are often ignored in the traditional multipole expansion. TD responses are difficult to be detected because they are covered by stronger electromagnetic effects[13]. However, TD response has been demonstrated from metamaterials composed of specially designed complex dielectric electromagnetic scatterers and also plays an important role in biological sensing [14,15], anapoles [16,17], nanomaterials [18-21], toroidal laser spacers [22], anapole nanolasers [23], photovoltaic devices [24], and other optical devices. In recent years, there are many metamaterial structures which can trigger TD responses, such as the wire structure of the toroidal metamolecule [25], multifold double-ring metamaterial [26], cavity-based metamaterial [27] , asymmetric double-bar metamaterial [28] and so on. It is particularly interesting to note that T. C. Huang et. al proposed an all-dielectric pentamer metamolecule consisting of nano-cylinders with two TD

resonances, whose frequencies, EM distributions and Q factor can be efficiently tuned due to the additional electric dipole mode [29]. J. Li et. al proposed a metamaterial structure comprising a periodic array of infinitely-long straight LiTaO3 microtubes and analyzed its far-field characteristic, transmittance, reflectance, and absorbance spectra [30].

A variety of nanoantennas including the Au-Ag core-shell, nanodisks, and nanoarrays have been proposed [31-34] and the spectral response of nanoantennas can be tuned and manipulated by optimizing the geometrical parameters of the nanostructures. The optical properties of dielectric nanoparticles such as nanospheres and nanodisks have received much attention in recent years, as the strong magnetic dipole (MD) response is most prominent in dielectric nanoparticles caused by retardation effects [35,36]. By engineering magnetic quadrupole (MQ) resonance of nanoparticles, metamaterials provide a versatile platform to study novel scattering phenomena [37]. Owing to the strong magnetic responses, dielectric nanoparticles have been used for directional antennas [38-42], broadband absorbers [43], and enhanced spectra [44].Therefore, much effort has been devoted to improving the magnetic excitation so that unidirectional propagation can be achieved in nanoantennas. So far, investigations on the excitations of toroidal dipole and magnetic multipoles resonances have predominantly focused on the visible and near-infrared spectral range over the years, there are increasing interests in the deep-ultraviolet (UV) wavelengths[45-51]. A potential advantage of UV plasmons is the high photon energy that can match the electronic transition energy of many organic molecules and solids. As described in this paper, a high-index all-dielectric nanostructure with four finite-length concentric cylinders is designed to achieve TD and magnetic multipole excitations (include MD and MQ excitations) by changing the direction of the same electric dipole emitters (EDs). The structure has great potential and the results described in this paper provide new information about the design of optical devices such as light nanoantennas and sensors.

2. Multipole composition method

We consider the scattering properties of various field modes of the high-index all-dielectric nanostructure using the multipole decomposition method and the resonant contributions from different multipoles are tuned to overlap spectrally [52]. Upon irradiation with incident light, the multipole moments of the scatterer are determined by polarization, where $P(r)=\varepsilon_0(\varepsilon_r-\varepsilon_d)E(r)$ is the polarization induced by the incident light wave in scattering , r is the radiation vector of the volume element in the scattering medium, ε_0 , ε_r , and ε_d represent the free-space dielectric constant, relative dielectric permittivity of the scatterer, and relative dielectric permittivity of the surrounding medium, respectively, and E(r) is the total electric field inside the scatterer. In order to clarify the contributions of different modes, multipole decomposition including the electric dipole moment P (ED), magnetic dipole moment M (MD), toroidal dipole moment T (TD), electric quadrupole moment Qe (EQ), and magnetic quadrupole moment Qm (MQ) are considered as follows [53].

$$P = \int P(r')dr' \tag{1}$$

$$M = -\frac{i\omega}{2}\int [r' \times P(r')]dr' \tag{2}$$

$$T = \frac{i\omega}{10}\int [(2r'^2 P(r') - (r' \cdot P(r'))r']dr' \tag{3}$$

$$Q^{e} = 3\int [r'P(r') + P(r')r']dr' \tag{4}$$

$$Q^{m} = -\frac{2i\omega}{3}\int [r' \times P(r')]r'dr' \tag{5}$$

It is noted that the multipoles locate at the origin of cartesian coordinate system according to the scatterer center of mass. Under this condition, the regular *ED* moment of the scatterer is given by Equation (1) where $P(r')$ is the polarization induced in the scatterer by an incident light wave and r' is the radius vector of a volume element inside the scattering medium.

Multipoles contributions indicate that the formants correspond to the overlap of several different multipole decomposition in the scattering field. The radiation power I from these different multipole moments is given by [54] and I_{inc} is the radiation power of the incident light wave.

$$I = \frac{1}{4\pi\varepsilon_0}[\frac{2\omega^4}{3c^3}|P|^2 + \frac{2\omega^4}{3c^3}|M|^2 + \frac{4\omega^5}{3c^4}\mathrm{Im}(P \cdot T^*) + \frac{2\omega^6}{3c^5}|T|^2 + \frac{\omega^6}{20c^5}|Q^e|^2 + \frac{\omega^6}{20c^5}|Q^m|^2] \tag{6}$$

$$C_{sca} = \frac{I}{I_{inc}} \tag{7}$$

3. Result and Discussion

Figure 1 describes a high-index all-dielectric nanostructure which consists of four finite-length concentric cylinders with a gap distance of $D=r_1-r_2$. The radius and height of the cylinder are R and h respectively, and d is the distance of the adjacent concentric cylinders.

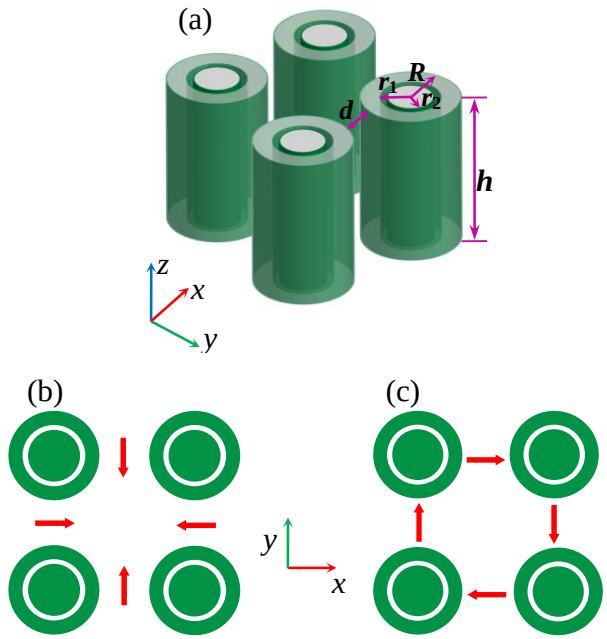

Fig. 1. Diagram of the all-dielectric nanostructure composed of four concentric cylinders with finite-length and high-index. The red arrows indicate the direction of the electric dipole emitter moment. *R*, *h*, and *d* are the radius, height, and gap between the cylinders. r_1, r_2 are the radius of two concentric cylinders. (a) Stereogram of the nanostructure, (b) TD excitation response, and (c) MD and MQ excitation response.

As shown in Fig.1(a), the high-index all-dielectric nanostructure with n=3.5 is surrounded by the medium with ε_d=1. The parameters are as follows: R=60 nm, r_1=40 nm, r_2=35 nm, and h=300 nm. First, the total electric field, magnetic field, and scattering modes scattering modes were calculated in this nanostructure by COMSOL multiphysics software based on the finite element method (FEM) under the excitation of the plane wave, as shown in Fig. 2. It is seen that TD keeps dominant in a much broader range from 230 nm to 430 nm, while the multipoles contributions to the scattering power are particularly weak. Therefore under the excitation of the plane wave, the TD and magnetic dipole can not achieve the desired enhancement effect.

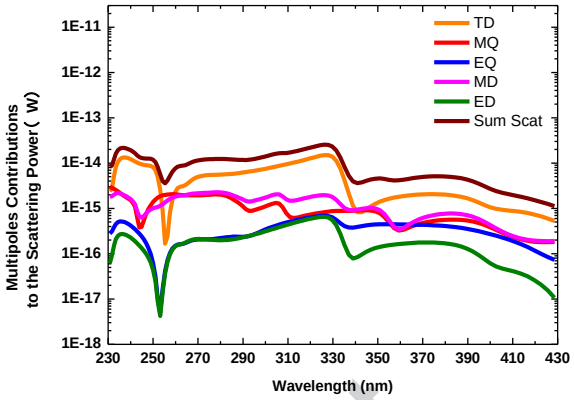

Fig. 2. Multipoles contributions to the scattering power under the excitation of the plane wave with cylinder radius R=60 nm, r_2=35 nm, r_1=40 nm, cylinder height h=300 nm, and d=20 nm.

Then, some electric dipole emitters with different directions shown by red arrows in Fig. 1(b) and 1(c) are placed on the bottom of the structure along the z direction, and the emission directions for the electric dipole emitters can be changed through the control of the phase difference between the induced magnetic and electric dipole modes of the antenna [55]. Under the excitation of these EDs, various excitation modes and radiation fields appear.

As the ED emitters are placed at the center of two adjacent cylinders and the directions of the four dipole emitters are shown in Fig. 1(b). The calculated TD (orange), MQ (red), EQ (blue), MD (pink), ED (green), and Sum Scat (Palm red) contributions to the scattering power are shown in Fig. 3. It is obvious that the contribution of the TD moment to the scattering power is dominated in the multipolar decomposition for the wavelength range between 230 nm and 430 nm. The contributions of the MD, MQ, ED, and EQ moments are weak. The maximum of the scattering power appears at a wavelength of 254 nm. Because of the contribution of EQ, the pure TD excitation does not appear at 254 nm, while the perfect TD excitation is observed at 312 nm.

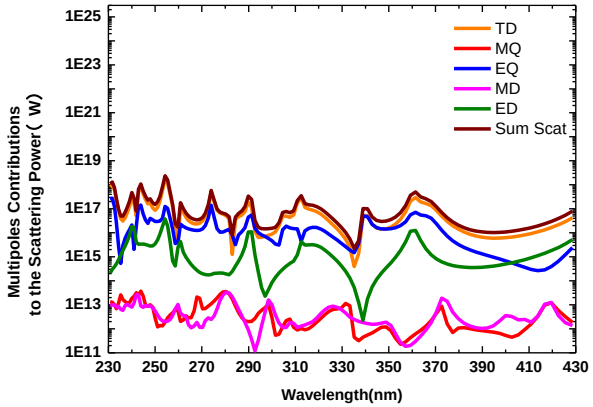

Fig. 3. Multipoles contributions to the scattering power with cylinder radius R=60 nm, r_2=35 nm, r_1=40 nm, cylinder height h=300 nm, and d=20 nm.

Figure 4 presents the near-field and far-field

distributions of the excitation and displacement currents density of the nanostructure at 254 nm. Figs. 4(a) and 4(c) show that the electric field pattern of each cylinder splits into four parts and two hot-spots can be observed from each part. The magnetic field diagram clearly shows two hot-spots in each cylinder as well as a distinct vortex which coils all four cylinders of the nanostructure as shown in Fig. 4(b). In this case, the induced magnetic field is confined into a well-defined annular region (marked by the red cones). The far-field radiation pattern can be seen in Fig. 4(d). The spatial location of the magnetic field and corresponding current mode are the key characteristics of TD excitation. The TD corresponds to currents flowing on the surface of a torus. The resonance excitation of the TD mode is caused by coupling of the magnetic modes of the four cylinders. The slight asymmetry of magnetic field or electric field distribution and displacement current is due to other multipolar excitations, most notably the electric quadrupole. Accordingly, the asymmetry of the displacement current (electric field) is caused by the superposition of the toroidal dipole and electric quadrupole and the appearance of the TD excitation is confirmed.

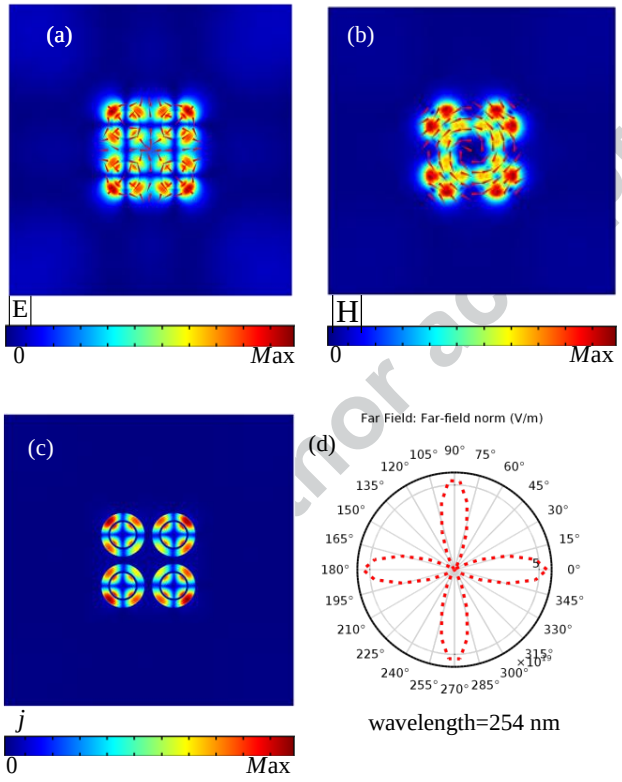

Fig. 4. (a) Electric field (absolute value|$\boldsymbol{E}$|), (b) Magnetic field (absolute value |$\boldsymbol{H}$|), and (c) Amplitude of the current density j. The red cones show instantaneous directions of the electric-field and magnetic-field distributions and (d) far-field scattering cross-sectional views on the x-y plane.

When the excitation moment directions of the four dipole emitters are changed in the clockwise direction as shown in Fig. 1(c), the calculated TD (orange), MQ (red), EQ (blue), MD (pink), ED (green), and Sum Scat (Palm red) contributions to the scattering power are displayed in Fig. 5. The contributions of MD and MQ play dominant roles in the wavelength range between 230 nm and 430 nm. The TD, EQ and ED multipoles contributions to the scattered power are weak. The dominant peak wavelength is 280 nm and the perfect MQ excitation is observed at 375 nm. Because of the contribution of MQ, the pure MD excitation does not appear, while MD excitation occupies the main position in the wavelength of 419 nm.

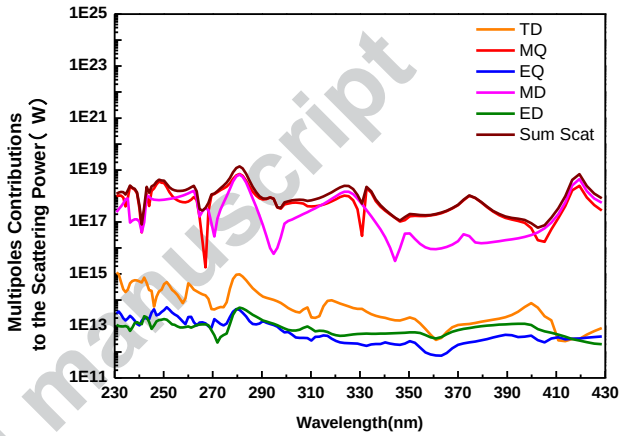

Fig. 5. Multipoles contributions to the scattering power with cylinder radius R=60 nm, r_2=35 nm,r_1=40 nm, cylinder height h=300 nm, and d=20 nm.

Figure 6 exhibits the near-field and far-field distributions of the excitation and currents density of the nanostructure at 419nm. From Fig .6(a), it is found that the electric field distribution is annular and the electric fields inside the gaps are parallel to the connecting lines of the cylinders (shown by the red cones). Fig. 6 (b) shows four circular spot patterns in the magnetic field highly concentrated in the center of the cylinder.

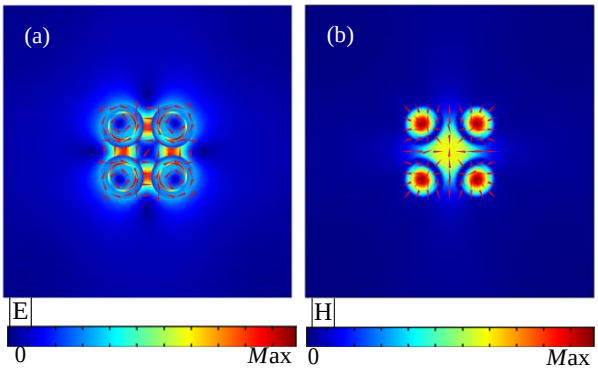

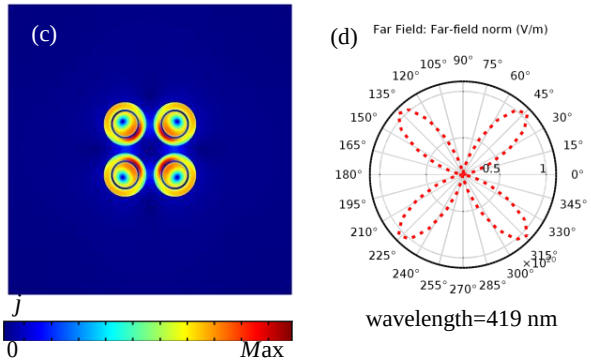

Fig. 6. The absolute values of the (a) electric field and (b) magnetic field at a wavelength of 419 nm. (c) The distribution of the current density *j* within the dielectric rods corresponds to the magnetic dipole response induced in the nanostructure. and (d) far-field scattering cross-sectional views on the x-y plane.

Figure 7 exhibits the near-field distributions of the excitation and currents density of the nanostructure at 375 nm. The electric field pattern of each cylinder splits into two parts and one hot-spots can be observed from each part in Figs. 7(a) and 7(c). Fig. 7(b) shows four circular spot patterns in the magnetic field highly concentrated in the outer corners of the cylinder. The distribution of the current density *j* corresponds respectively to the MD and MQ response induced in the nanostructure as shown in Fig. 6(c) and Fig. 7(c). MD and MQ radiation pattern are also confirmed in Fig. 6(d) and Fig. 7(d). These results clearly demonstrate the appearance of MD and MQ excitation responses.

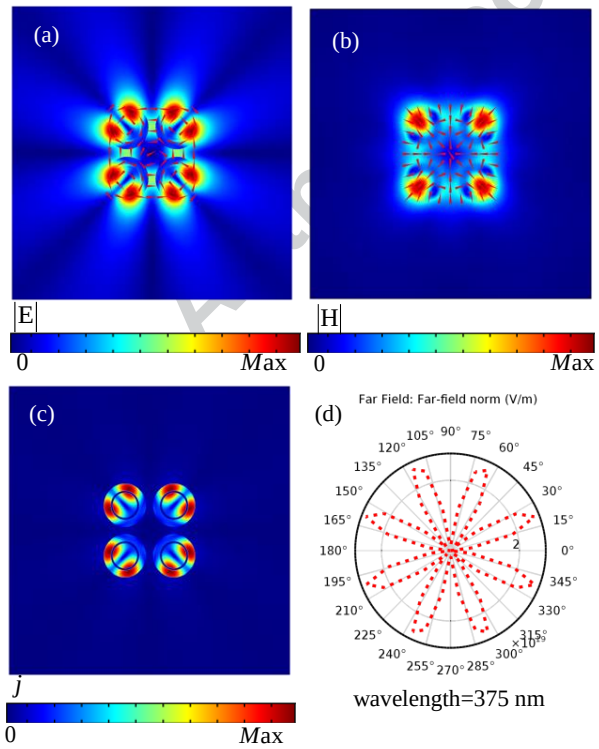

Fig. 7. The absolute values of the (d) electric field and (e) magnetic field at a wavelength of 375 nm. (c) The distribution of the current density j within the dielectric rods corresponds to the magnetic quadrupole response induced in the nanostructure. (d) far-field scattering cross-sectional views on the x-y plane.

The phenomena mentioned above are only applicable to the determination of structural parameters. Actually, if the parameters of the nanostructure are changed, we can always get the excitation response of TD and magnetic excitation. The excitation response of MQ and MD with various gap distances (*D*) is presented in Figs. 8 (a) and 8 (b), respectively. With regard to MQ excitation in Fig. 8 (a), the spectral response with *D*=10 nm (red), 5 nm (blue) and 2 nm (green) is shown and the total summed scattering is indicated by short dashed lines for comparison. The other geometric parameters of the nanostructure are *h*=300 nm and *d*=20 nm. As shown in Fig. 8 (a), the excitation response intensity of the MQ moment weakens gradually with decreasing D and near-pure MQ excitation response is observed at 237 nm and 360 nm for *D*=10 nm. The response of MD excitation for *D*=10 nm (pink) , 5 nm (violet) and 2 nm (dark cyan) is shown in Fig. 8 (b). The MD excitation response is observed at 281 nm and 419 nm for *D*=5 nm and at 299 nm and 377 nm for *D*=2 nm. Owing to the contribution of MQ excitation, the perfect MD excitation does not appear at these wavelengths.

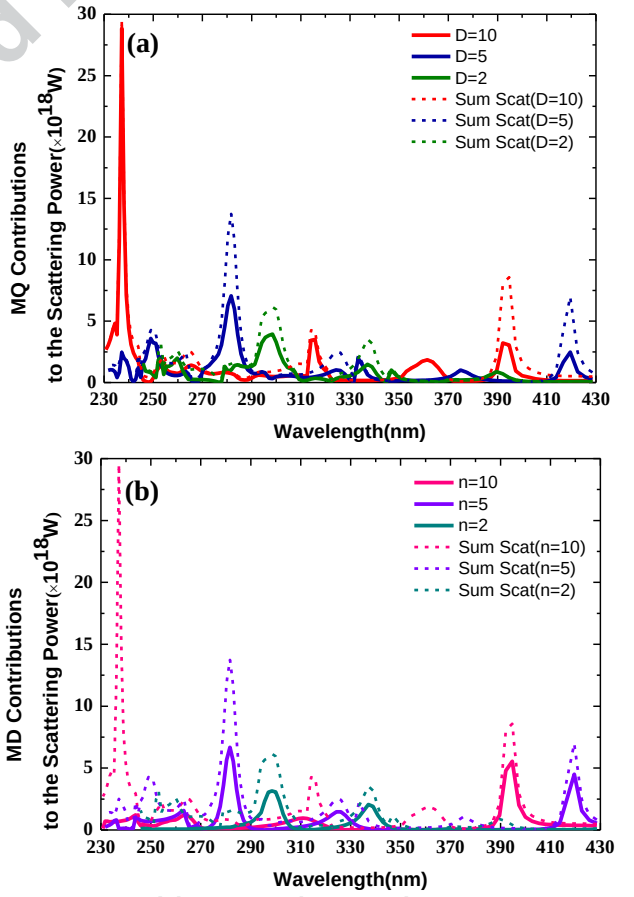

Fig. 8. (a) MQ and (b) MD contributions to the scattering power as a function of wavelength for different gaps between r_1 and r_2 while keeping *h*=300 nm and *d*=20 nm.

Figure 9 shows the TD contribution to the scattering power for *h*=250 nm and 200 nm while the other geometric parameters of the nanostructure are set as *R*=60 nm and *d*=20 nm. The near-pure TD resonance excitation can always be observed from the UV-light region for different structural parameters. The TD and magnetic multipoles excitations can be obtained in the UV region by designing the nanostructure with the proper geometric parameters and these phenomena are obtained by adjusting the excitation direction of the electric dipole emitters.

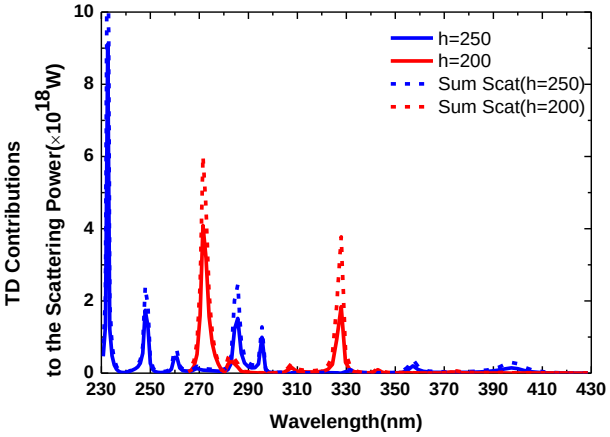

Fig. 9. TD contribution to the scattering power as a function of wavelength for different *h* while keeping *D* =5 nm and *d* =20 nm.

4. Conclusion

A novel nanostructure with different directions of electric dipole emitters is designed and the scattering properties of the various field modes are demonstrated by the multipole composition method. TD, MQ and MD excitations are observed in the UV region but other multipoles modes are suppressed. Considering that the TD, MQ and MD modes have strong correlation with the local near-field distribution and far-field scattering modes, the excitations of the TD and magnetic multipoles modes provide new information and ideas about light nanoantennas and spectroscopy.

Funding Information: Natural Science Foundation of Heilongjiang Province [E2017010]; Provincial talent project [ts26180221]; Northeast Petroleum University Innovation Foundation For Postgraduate [YJSCX2017-034NEPU]; City University of Hong Kong Strategic Research Grant (SRG) [7005105].

Disclosures. The authors declare no conflicts of interest.

References

[1] C. Liu, W. Q. Su, F. M. Wang, X. L. Li, L. Yang, T. Sun, H.W. Mu, P. K. Chu: J. Mod. Opt. **66,**1-6 (2019).
[2] Z. Yi, C.P. Liang, X.F. Chen, Z.G. Zhou, Y.J. Tang, X. Ye, Y.G. Yi, J.Q. Wang, P.H. Wu: Micromachines, **10** (7), 443 (2019).
[3] X. X. Wang, J. K. Zhu, X. L. Wen, X. X. Wu, Y. Wu, Y. W. Su, H. Tong, Y. P. Qi, H. Yang: Opt. Mater. Express, **9** (7), 3079-3088 (2019).
[4] C. Liu, Y. Lin, X. L. Lu, Q. Liu, F. M. Wang, J. W. Lv, T. Sun, H.W. Mu, P. K. Chu: Opt. Express, **25**, 14227-14237 (2017).
[5] C. L. Cen, Y. B. Zhang, C. P. Liang, X. F. Chen, Z. Yi, T. Duan, Y. J. Tang, X. Ye, Y. Yi, S. Xiao: Phys. Lett. A . **383**, 3030–3035 (2019).
[6] X. X. Wang , X. X. Wu , J. K. Zhu , Z. Y. Pang , H. Yang ,Y. P. Qi: Sensors, **19** (5), 1187 (2019).
[7] L. Liu, L. Ge, P. Hu, H. Xiang, W. Yang, Q. Liu , D. Han: J. Phys. D: Appl. Phys. **51** (3), 035106 (2018).
[8] M. Kläui, C. A. F. Vaz, L. Lopez-Diaz, J. A. C. Bland: J. Phys. Condens. Matter **15**, R985 (2003).
[9] I. I. Naumov, L. Bellaiche ,H. X. Fu: Nature, **432**, 737 (2004).
[10] Y. V. Kopaev: Phys. Usp. **52**,1111 (2009).
[11] L. Ungur, S. K. Langley, T. N. Hooper, B. Moubaraki, E. K.Brechin, K. S. Murray,L. F. Chibotaru: J. Am. Chem. Soc. **134**, 18554(2012).
[12] W. Liu, J. Zhang, B. Lei, H. Hu, A. E. Miroshnichenko: Opt. Lett.**40**, 2293 (2015).
[13] A. A. Basharin, M. Kafesaki, E. N. Economou, C. M. Soukoulis, V. A. Fedotov, V. Savinov, N. I. Zheludev: Phys. Rev. **X5**,011036 (2015).
[14] A. V. Kabashin, P. Evans, S. Pastkovsky, W. Hendren, G. A. Wurtz,R. Atkinson, R. Pollard, V. A. Podolskiy, A. V. Zayats: Nat. Mater. **8**, 867 (2009).
[15] R. Wang , N. L. Dal: Opt. Express, **24**, 19048 (2016).
[16] N. A. Nemkov, I. V. Stenishchev, A. A. Basharin: Sci. Rep. **7**, 1064 (2017).
[17] P. Muhlschlegel, H. J. Eisler, O. J. F. Martin, B. Hecht, and D. W. Pohl: Science, **308**, 1607 (2005).
[18] T. Pakizeh, M. Kall: Nano Lett. **9**, 2343 (2009).
[19] B. Rolly, B. Stout, N. Bonod: Opt. Express **20**, 20376 (2012).
[20] L. K. Warne, L. I. Basilio, M. B. Sinclair, S. Campione: Opt. Express **23**, 2293 (2015).
[21] P. D. Terekhov, K. V. Baryshnikova, A. S. Shalin, A. Karabchevsky, and A. B. Evlyukhin: Opt. Lett. **42**, 835 (2017).
[22] Y. W. Huang, W. T. Chen, P. C. Wu, V. A. Fedotov, N. I. Zheludev, D. P. Tsai: Sci. Rep. **3**, 1237 (2013).
[23] J. S. T. Gongora, A. E. Miroshnichenko, Y. S. Kivshar, A. Fratalocchi: Nat. Commun. **8**, 15535 (2017).
[24] H. A. Atwater, A. Polman: Nat. Mater. **9**, 865 (2010).
[25] Kaelberer, V. A. Fedotov, N. Papasimakis, D. P. Tsai, N. I. Zheludev: Science, **330** (6010), 1510–1512 (2010).

[26] Z.-G. Dong, P. Ni, J. Zhu, X. Yin, X. Zhang: Optics Express, **20**(12) (2012).

[27] Z.-G. Dong, J. Zhu, X. Yin, J. Li, C. Lu , X. Zhang: Physical Review B, **87** (24) (2013).

[28] Z.-G. Dong, J. Zhu, J. Rho, J.-Q. Li, C. Lu, X. Yin, X. Zhang: Applied Physics Letters, **101** (14), 144105 (2012).

[29] T. C. Huang, B. X. Wang, C. Y. Zhao: Journal of Applied Physics, **125** (9), 093102 (2019).

[30] J. Li , J. Shao , Y.-H. Wang, M.-J. Zhu , J.-Q. Li, Z.-G. Dong: Optics Express, **23** (22), 29138 (2015).

[31] C. Liu, J. V. Lv, Z. Liu , S. Zheng, Q. Liu, T. Sun, P. K. Chu: Plasmonics, **11** (6), 1589–1595 (2016).

[32] J.V. Lv, H.W. Mu, Q. Liu, X. Zhang , X. Li, C. Liu, P. K. Chu: Appl Optics, **57**(17), 4771(2018).

[33] H. Tong, Y. Q. Xu, Y.W. Su, X. X. Wang: Results Phys.**14**, 102460 (2019).

[34] X. X. Wang, J. K. Zhu, H. Tong, X. D. Yang, X. X. Wu, Z. Y. Pang, H. Yang, Y. P. Qi: Chin. Phys. B, **28** (4), 044201 (2019).

[35] A. B. Evlyukhin, C. Reinhardt , A. Seidel , B. S. Luk'yanchuk, B. N. Chichkov: Phys. Rev. B. **82**, 045404 (2010).

[36] A. B. Evlyukhin, R.L. Eriksen, W.Cheng, J. Beermann , C. Reinhardt, A. Petrov, S. Prorok, M. Eich, B. N. Chichkov, S. I. Bozhevolnyi: Sci. Rep. **4**, 4126 (2014).

[37] T. G. Habteyes, I. Staude, K. E. Chong, J. Dominguez, M. Decker, A. Miroshnichenko, Y. Kivshar, and I. Brener: ACS Photonics, **1**, 794-798 (2014).

[38] M. K. Schmidt, R. Esteban, J. J. Saenz, I. Suarez-Lacalle, S. Mackowski, J. Aizpurua: Opt. Express. **20**, 13636-13650 (2012).

[39] A. Garcia-Etxarri, R. Gomez-Medina, L. S. Froufe-Perez, C. Lopez, L. Chantada, F. Scheffold, J.Aizpurua, M. Nieto-Vesperinas, J. J. Saenz: Opt. Express. **19**, 4815-4826 (2011).

[40] J.van de Groep, A. Polman: Opt. Express. **21**, 26285-26302 (2013).

[41] I. Staude, A. E. Miroshnichenko, M. Decker, N. T. Fofang, S. Liu, E. Gonzales, J. Dominguez, T. S. Luk, D. N. Neshev, I. Brener, and et al: ACS Nano.**7**,7824-7832 (2013).

[42] A. E. Krasnok, C. R. Simovski, P. A. Belov, Y. S.Kivshar: anoscale. **6**, 7354-7361 (2014).

[43] P. Spinelli, M. A. Verschuuren, A. Polman: Nat. Commun. **3**, 692 (2012).

[44] P. Albella, M. A. Poyli, M. K. Schmidt, S. A. Maier, F. Moreno, J. J. Saenz, J. Aizpurua: J. Phys.Chem. C. **117**, 13573-13584 (2013).

[45] L. Ge, L. Liu, S. Dai, J. Chai, Q. Song, H. Xiang, D. Han: Optics Express, **25** (10), 10853 (2017).

[46] D. V. Nesterenko, Z. Sekkat: Plasmonics, **8** (4), 1585–1595 (2013).

[47] M. Rodriguez, C. Furse, J. S. Shumaker-Parry, S. Blair: ACS Photonics, **1** (6), 496–506 (2014).

[48] D. Hasan, C. P. Ho, P. Pitchappa, C. Lee: ACS Photonics, **2** (7) , 90–898 (2015).

[49] M. B. Ross, G. C. Schatz: The Journal of Physical Chemistry C, **118** (23), 12506–12514 (2014).

[50] Z. Lin , X. Wang , J. Liu , Z. Tian, L. Dai, B. He, Z. Hu: Nanoscale, **7** (9), 4114–4123 (2015).

[51] J. Hu, L. Chen, Z. Lian, M. Cao, H. Li , W. Sun, H. Zeng: The Journal of Physical Chemistry C, **116** (29), 15584–15590 (2012).

[52] Q. Zhang, J. J. Xiao, M. L. Li, D. Z. Han, L. Gao: ACS Photonics, **2**, 60-65 (2015).

[53] A. B. Evlyukhin, T. Fischer, C. Reinhardt, B. N. Chichkov: Phys. Rev. B **94**, 205434-1–8 (2016).

[54] X. L. Zhang, S. B. Wang, Z. F. Lin, H. B. Sun, C. T. Chan: Phys. Rev. B **92**, 043804-1–8 (2015).

[55] T. Feng, W. Zhang, Z. Liang, Y. Xu: Journal of Physics: Condensed Matter, **30**(12), 124002(2018).